Data-driven honeybee antennal lobe model suggests how stimulus-onset asynchrony can aid odour segregation

Article (Unspecified)

Data-driven honeybee antennal lobe model suggests how stimulus-onset asynchrony can aid odour segregation

Thomas Nowotny[a], Jacob S. Stierle[b], C. Giovanni Galizia[b], Paul Szyszka[b]

[a] *Centre for Computational Neuroscience and Robotics, School of Engineering and Informatics, University of Sussex, Falmer, Brighton BN1 9QJ, UK*
[b] *Fachbereich Biologie, Universität Konstanz, Universitätstraße 10, 78457 Konstanz, Germany*

Abstract

Insects have a remarkable ability to identify and track odour sources in multi-odour backgrounds. Recent behavioural experiments show that this ability relies on detecting millisecond stimulus asynchronies between odourants that originate from different sources. Honeybees, *Apis mellifera*, are able to distinguish mixtures where both odourants arrive at the same time (synchronous mixtures) from those where odourant onsets are staggered (asynchronous mixtures) down to an onset delay of only 6 ms. In this paper we explore this surprising ability in a model of the insects' primary olfactory brain area, the antennal lobe. We hypothesise that a winner-take-all inhibitory network of local neurons in the antennal lobe has a symmetry-breaking effect, such that the response pattern in projection neurons to an asynchronous mixture is different from the response pattern to the corresponding synchronous mixture for an extended period of time beyond the initial odourant onset where the two mixture conditions actually differ. The prolonged difference between response patterns to synchronous and asynchronous mixtures could facilitate odour segregation in downstream circuits of the olfactory pathway. We present a detailed data-driven model of the bee antennal lobe that reproduces a large data set of experimentally observed physiological odour responses, successfully implements the hypothesised symmetry-breaking mechanism and so demonstrates that this mechanism is consistent with our current knowledge of the olfactory circuits in the bee brain.

Keywords: Olfactory system, mixtures, computational model, stimulus asynchrony, odour object recognition, odour segregation

Email address: t.nowotny@sussex.ac.uk (Thomas Nowotny)
URL: http://www.sussex.ac.uk/Users/tn41 (Thomas Nowotny)

1. Introduction

Airborne odourants distribute in turbulent odour-plumes that fluctuate at multiple temporal scales, spanning from milliseconds to minutes (Murlis et al., 1992; Riffell et al., 2009). In a natural environment the odour-plumes of a variety of odour sources intermingle. In order to form a meaningful perception of the olfactory landscape, animals need to segregate concurrent odours from independent sources within this mixture. Generally, odourants that are emitted together from one odour source will travel together in the same odour filaments while compounds emitted from other sources will arrive in separate filaments at the sensory organs. The temporal relationships between odourant stimulus onsets thus contains information about whether the odourants belong to the same or a different odour source (Hopfield, 1991).

Insects possess a remarkable ability to segregate odourants from different sources based on the exact timing of the onset of concurrent odour stimuli. In honeybees, a 6-millisecond temporal difference in stimulus onset is sufficient to segregate an odour-object from a mixture (Szyszka et al., 2012). Moth and beetles can distinguish blends of attractive pheromones with antagonistic odours in which the components arrive at the same time (synchronous mixture), from blends of the same substances where the components arrive with temporal differences (asynchronous mixture): In asynchronous mixtures the antagonistic effect of the additional odour becomes weaker as soon as the arrival of the mixture components is separated by only one or a few milliseconds (Baker et al., 1998; Andersson et al., 2011).

Two previous studies, in locusts and honeybees, have shown that central olfactory neurons are sensitive to odour-onset asynchrony: their responses to mixtures partly match those evoked by the individual components if the onsets of the stimuli differ (Broome et al., 2006; Stierle et al., 2013). In particular, differences in responses were found in the projection neurons (PNs) of the antennal lobe (AL), the first relay of olfactory information in the insect brain. The AL is subdivided into smaller spherical areas called glomeruli. In *Drosophila* olfactory receptor neurons (ORNs) with the same receptor protein converge onto the same glomerulus, and thus provide every glomerulus with a distinct response profile (Vosshall et al., 2000). We will here assume the same connectivity pattern for the bee. Within the AL, a network of intra- and inter-glomerular inhibitory local neurons (LNs) and excitatory local neurons has been found to be involved in odour processing in the fly (Olsen et al., 2007; Shang et al., 2007; Silbering and Galizia, 2007; Silbering et al., 2008) and the bee (Sachse and Galizia, 2002). It is however currently unknown how the AL network contributes to odour segregation based on millisecond stimulus onset-asynchrony. In this paper we investigate the hypothesis that the network of inhibitory LNs in the AL could aid distinguishing asynchronous mixtures and synchronous mixtures of odours. The fundamental idea can be thought of as a symmetry-breaking effect of a winner-take-all

LN network: Assuming that for two given odourants A and B there are two different response patterns in ORNs and hence two different "winning" activity patterns in the network of LNs, say LN_A and LN_B, and potentially a third pattern for the synchronous mixture AB of A and B, say LN_{AB}. Then, if an asynchronous mixture A-t-B of A, t ms delay, then B arrives at the antenna, the initial activation by odourant A will activate pattern LN_A, which will inhibit other LN activity patterns, such that when odourant B arrives, the pattern LN_A remains active and the response appears different from the response to the synchronous mixture AB where pattern LN_{AB} is active. The same reasoning applies to the asynchronous mixture B-t-A.

We test our hypothesis in a detailed model of the honeybee AL, using a large data set from the literature (Ditzen, 2005; Strauch et al., 2012) to calibrate the responses to 16 odourants that we then use to make predictions for the responses to their synchronous and asynchronous mixtures.

2. Methods

In this paper we investigate a model of the honeybee early olfactory pathway. We implemented the model using the typical rules for the olfactory system: Each ORN expresses only one type of receptor and ORNs of the same type connect to the same glomerulus. The detailed connectivity of the model is given below. In order to obtain realistic receptor responses to mixtures, we implemented a rate description of binding, unbinding, activation and inactivation of receptors which implements a syntopic mixture model that has been found to be accurate for many observations in bee olfaction (Münch et al., 2013). We then generate Poisson spike trains from the receptor activation data to take account of the known unreliability of ORNs. The output of the ORN population feeds into an AL model of PNs and LNS implemented with Hodgkin-Huxley type conductance based neuron models which were tuned to reproduce the electrophysiological data obtained in honeybees (Krofczik et al., 2008). One of the larger unknowns in the model are the activation of different receptor types in response to different odours. To obtain an estimate of the binding and activation rates, we used an indirect parameter estimation that matched the activation patterns of the AL to experimental data (Ditzen, 2005) by adjusting the activation rates on the level of the receptors (see "Bootstrapping" below). In order to relate our spiking neuronal network output to the experimental data from calcium imaging experiments we employed spike density functions (SDFs). We then used correlation analysis of glomerular activation patterns in terms of averaged SDFs of PNs to analyse the simulation results with respect to the question of odour segregation.

The details of each of the model elements and analysis methods are explained in the following sub-sections.

2.1. Spike density functions

We used SDFs as a proxy of the Ca^{2+} signal observed in experiments. SDFs were calculated by convolving the spike trains with the asymmetric kernel

$$k(\hat{t}) = \hat{t} \exp\Big(- \frac{\hat{t}}{\tau}\Big) \tag{1}$$

where $\hat{t} = t - t_{\text{spike}} + \tau$, so that the maximum of k is situated at the occurrence of the spike, t_{spike}. The timescale of the kernel was chosen as $\tau = 50$ ms.

2.2. Olfactory receptors

We describe olfactory transduction in ORNs as odourant binding and unbinding at olfactory receptors comprising a set of reactions from unbound receptors R to bound receptor-odourant complexes R_i to activated bound complexes R_i^*, where $i = A, B, \ldots$ labels the different odourants. For odourants A, B, ... present at a population of receptors we have the corresponding rate equations

$$\dot{r}_i = k_{1,i}^+ r(c_i)^n + k_{2,i}^- r_i^* - k_{1,i}^- r_i - k_{2,i}^+ r_i \tag{2}$$

$$\dot{r}_i^* = k_{2,i}^+ r_i - k_{2,i}^- r_i^* \tag{3}$$

for each odourant i and

$$\dot{r} = \sum_{i \in OD} k_{1,i}^- r_i - k_{1,i}^+ r(c_i)^n \tag{4}$$

for the free receptor, where $OD = \{A, B, \ldots\}$ denotes the set of odourants that are present. The lower case variables r, r_i, and r_i^* denote the fraction of receptors that are in the states R (unbound), R_i (bound to odourant i) and R_i^* (bound to odourant i and activated). c_i denotes the concentration of odourant i. The parameters $k_{1,i}^+$, $k_{1,i}^-$, $k_{2,i}^+$ and $k_{2,i}^-$ are rate constants describing the rate with which odourants bind and unbind ($k_{1,i}^+$, $k_{1,i}^-$) and bound receptors activate and inactivate ($k_{2,i}^+$, $k_{2,i}^-$). For a single odourant A and in steady state, the above equations lead to Hill activation functions for odour responses as a function of odour concentration (Rospars et al., 2008).

Assuming this underlying model for the odourant receptors and using the calcium imaging data of odour responses to odourant-concentration series published in Ditzen (2005), we fit the rate constants $k_{1,i}^+$, $k_{1,i}^-$, $k_{2,i}^+$ and $k_{2,i}^-$ so that the resulting Hill curves of stationary activation approximate the experimentally observed activation levels of each glomerulus in response to each odourants at the four measured concentrations of 10^{-4}, 10^{-3}, 10^{-2} and 10^{-1} dilution. The resulting parameter estimates disregard any transmission or network effects in the antennal lobe by equating average PN activity (measured by Ca^{2+} imaging) with the activation level of the corresponding receptor type and are hence likely not very accurate. They provide us, however, with a starting point from which we can bootstrap our simulations to iteratively approximate the biological system better.

2.3. Bootstrapping

Using the initial guesses for the activation curves of receptor types for each of the 16 used odourants, we generate the network output in a forward simulation of the system (see "Network model" and "Simulation" below). We interpret the spike density function averaged over the population of PNs in each glomerulus as a proxy for the Ca^{2+} activation of the glomerulus observed in experiments. We then compare the activity levels observed in the model with the target values from the experimental data and adjust the target activation of the corresponding receptor types proportionally to this mismatch. We re-fit the rate parameters of the binding reactions to these adjusted activation levels as described in "Receptor model" above and re-iterate the process of simulation and re-fitting until a satisfactory match between model PN SDFs and experimental Ca^{2+} activation was found.

We observed that there were many different sets of kinematic parameters that were similarly good for reproducing the data, i.e. there are many local minima in the fitness landscape of this optimisation problem. We eventually chose one set of parameters as the best fit and performed most of the numerical work with this set. As a simple control we then repeated parts of the numerical experiments with a different, similarly good parameter set and compared the observations in both cases (see Results section).

The indirect estimation of the rate parameters of receptor dynamics used here is only meaningful as an estimate of the ratio of binding and unbinding and activation and inactivation rates, as we are approximating the Hill curve of steady state activation that depends only on those ratios (Rospars et al., 2008). However, with this caveat in mind we believe that the approach is meaningful even though the receptor kinetics are on a much faster timescale than the experimental Ca^{2+} data used to constrain them.

2.4. Olfactory receptor neurons

To generate realistic spiking olfactory receptor neurons (ORNs) we translate the fraction of activated receptors into the spike rate of a Poisson process using an appropriate rescaling factor,

$$\lambda = \lambda_{\max} \rho \sum_{i \in OD} r_i^*, \tag{5}$$

where $\lambda_{\max} = 0.0625$ kHz and ρ describes a process of spike rate adaptation, i.e., a gradual decrease of the ORN spike rate over the duration of a stimulus. The dynamics of ρ are described by

$$\dot{\rho} = -\alpha_{\text{sra}} \lambda \rho + \beta_{\text{sra}} (1 - \rho) \tag{6}$$

where the rate constants of adaptation and recovery are $\alpha_{\text{sra}} = 0.004$ kHz and $\beta_{\text{sra}} = 0.002$ kHz. This implements dynamics in which ρ is driven to

0 for large spiking frequencies λ, hence effectively reducing λ, and recovers back to 1 when λ is small and hence the second term dominates.

In practice the Poisson process with λ is approximated neglecting the probability for more than one spike in each (small) integration time step and thus using

$$p_{\text{spike}} = \lambda \Delta t \tag{7}$$

for the probability of a spike to occur within an integration time step Δt. Spikes have a nominal width of one time step or 1 μs, whichever is longer and are refractory for another μs. Note that these values are only of technical relevance for the simulation as the synapse model does not depend on the spike width and the spike rates of the ORNs are sufficiently low so that a spike occurrence within the timescale of the refractory period has practically probability 0. The ORNs have a baseline firing rate of 0.2 Hz in absence of any stimulation.

2.5. Projection and local neurons

The PNs and LNs are described by a Hodgkin-Huxley model (Buckley and Nowotny, 2011; Nowotny and Rabinovich, 2007) modified from (Traub and Miles, 1991) and the LNs additionally exhibit spike rate adaptation (Krofczik et al., 2008), as in (Buckley and Nowotny, 2011) implemented by an M-type current,

$$C\dot{V}_i = -I_{\text{Na}} - I_{\text{K}} - I_{\text{L}} - I_{\text{M}} - I_{i,\,\text{DC}} - I_{i,\,\text{syn}}, \tag{8}$$

where $I_{i,DC}$ is a constant bias current regulating the intrinsic excitability of neurons. The leak current is $I_L = g_L(V_i - E_L)$ and the ionic currents I_{Na} and I_{K} are described by

$$\begin{aligned} I_{\text{Na}}(t) &= g_{\text{Na}} m_i(t)^3 h_i(t)(V_i(t) - E_{\text{Na}}) \\ I_{\text{K}}(t) &= g_{\text{K}} n_i(t)^4 (V_i(t) - E_{\text{K}}) \\ I_{\text{M}}(t) &= g_{\text{M}} z_i(t)(V_i(t) - E_{\text{K}}). \end{aligned} \tag{9}$$

The synaptic current I_{syn} to each neuron is the linear sum of all synapses onto the neuron, each synaptic current given by (14). Each activation and inactivation variable $y_i(t) = \{m_i(t), h_i(t), n_i(t), z_i(t)\}$ satisfies first-order kinetics

$$\frac{dy_i(t)}{dt} = \alpha_y(V_i(t))(1 - y_i(t)) - \beta_y(V_i(t))y_i(t), \tag{10}$$

with non-linear functions $\alpha_y(V)$ and $\beta_y(V)$ given by

$$\begin{aligned}
\alpha_m &= 0.32\text{kHz}(-52-v)/(\exp((-52-v)/4)-1)\\
\beta_m &= 0.28\text{kHz}(25+v)/(\exp((25+v)/5)-1)\\
\alpha_h &= 0.128\text{kHz}\exp((-48-v)/18)\\
\beta_h &= 4\text{kHz}/(\exp((-25-v)/5)+1)\\
\alpha_n &= 0.032\text{kHz}(-50-v)/(\exp((-50-v)/5)-1)\\
\beta_n &= 0.5\text{kHz}\exp((-55-v)/40)\\
\alpha_z &= 0.0025\text{kHz}/(1+\exp((20-v)/5))\\
\beta_z &= 0.0001kHz
\end{aligned} \tag{11}$$

where $v = V/[mV]$. The remaining parameter values are $C = 0.143$ nF, $g_L = 0.02672$ μS, $E_L = -63.563$ mV, $g_{\text{Na}} = 7.15$ μS, $E_{\text{Na}} = 50$ mV, $g_{\text{K}} = 1.43$ μS, $E_{\text{K}} = -95$ mV as in Buckley and Nowotny (2011). The parameters $I_{i,\,\text{DC}} = 0.06$ nA for PNs and $I_{i,\,\text{DC}} = -0.03$ nA for LNs and $g_M = 0$ for PNs and $g_M = 0.006$ μS for LNs were chosen to reproduce a realistic baseline firing rate for PNs of about 20 Hz and to otherwise qualitatively match the intra-cellular measurements of PN and LN activity reported in Krofczik et al. (2008).

2.6. Synapses

Synapses are described by first order kinetics (Destexhe et al., 1994) according to

$$\dot{r} = -\gamma r + \delta(t_{\text{spike}}) \tag{12}$$

$$\dot{s} = \alpha(r-s) - \beta s \tag{13}$$

$$I_{\text{syn}} = g_{\text{syn}} s (V_{\text{post}} - V_{\text{rev}}), \tag{14}$$

where the reversal potential V_{rev} is 0 mV for excitatory and -80 mV for inhibitory synapses and $\delta(.)$ denotes the delta distribution, i.e. $\delta(t) = 0$ for $t \neq 0$ and $\int \delta = 1$. The rate constants are $\alpha = 0.1$ kHz for ORN to PN synapses, $\alpha = 0.5$ kHz for all other synapses, $\beta = 0.01$ kHz for ORN to PN or to LN connections, $\beta = 0.05$ kHz for LN to PN connections, $\beta = 0.02$ kHz for LN to LN connections and $\gamma = 0.25$ kHz for all synapses.

2.7. Network model

The antennal lobe (AL) network model is depicted in figure 1. In brief, ORNs project to both PNs and LNs in the AL with excitatory synapses, each group of 600 ORNs of a given type to the corresponding glomerulus of 5 PNs and 1 LN. The number of PNs in the model was based on the commonly cited cell count of about 800 PNs in the AL of bees (Rybak, 1994; Hammer, 1997). The number of LNs in the AL of bees has been estimated to be about 4000 (Witthöft, 1967) and many different types of LNs

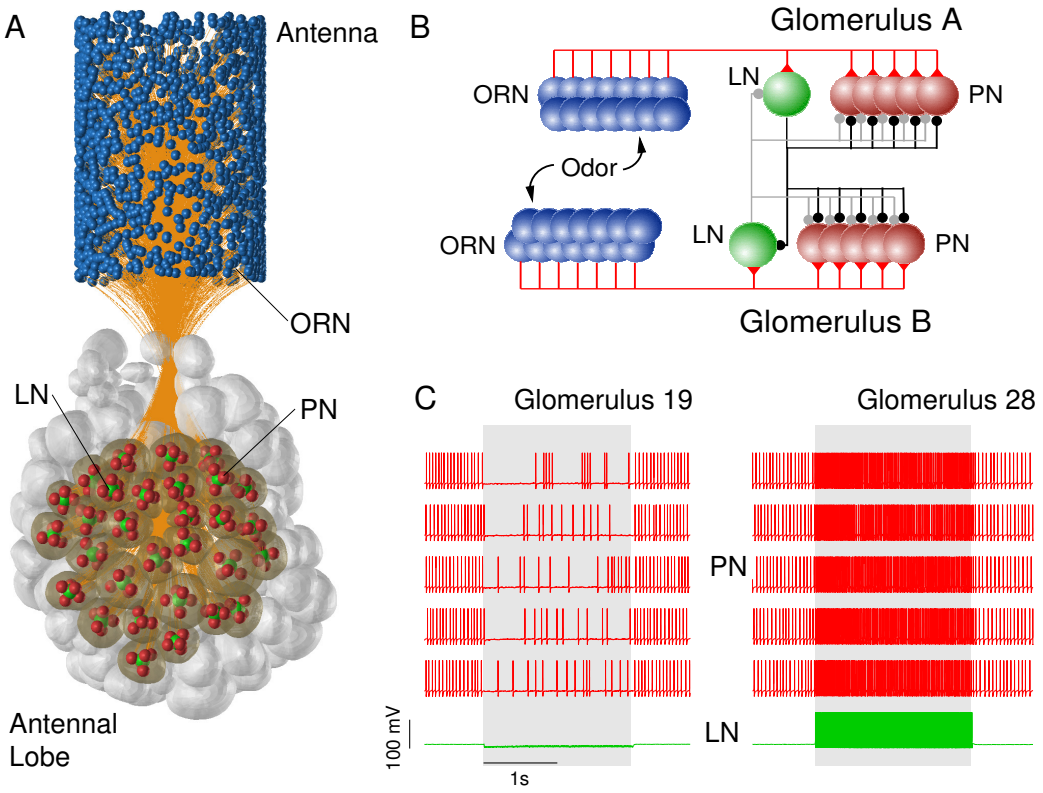

Figure 1: Illustration of the network model. A) anatomical arrangement of the modelled neuronal network. ORNs on the antenna are depicted as blue spheres, the glomeruli of the AL were derived from the 3D AL atlas (Galizia et al., 1999) and each glomerulus for which we had sufficient data (transparent) is modelled with 5 PNs (red spheres) and one LN (green spheres). B) Functional network architecture. ORNs of the same type converge onto one common glomerulus in which they excite all PNs and the LN. The LN of each glomerulus inhibits all PNs of the same glomerulus and of other glomeruli. The strength of inhibition was chosen proportional to the correlation of PN activity of the glomeruli as observed in the data. The LNs also inhibit each other, forming a winner-take-all circuit (see main text). C) Example voltage traces of PNs and LNs from glomerulus 19 and 28 in response to hexanol. The odour stimulus is present during the time indicated by the grey area.

have been reported (Abel et al., 2001), both with respect to their anatomy (uni-glomerular, inter-glomerular, multi-glomerular) and their transmitters ($GABA_A$, $GABA_B$, histamine, glutamate/chloride, ...), see Galizia (2008) for review. Furthermore, recent work in *Drosophila* has also discovered excitatory local neurons Olsen et al. (2007) that form gap junctions within the AL Huang et al. (2010); Yaksi and Wilson (2010). In the model presented here we only model multi-glomerular inhibitory LNs which are assumed to form $GABA_A$ synapses throughout the entire AL. This choice was guided by our hypothesis of a winner-take-all LN network. The exact number of such neurons is not known and for simplicity we hence only modelled the minimally necessary number of one for each glomerulus that will support our hypothesised WTA network. We have shown in previous work Zavada et al. (2011) that in terms of modelling, extending the WTA network to groups of LNs for each glomerulus is unproblematic and leads to comparable results.

Synaptic conductances were $g_{\text{syn}} = 0.48$ nS for ORN to PN connections and $g_{\text{syn}} = 0.16$ nS for ORN to LN connections. The LNs inhibit all other LNs with $g_{\text{syn}} = 150$ nS and the PNs of all glomeruli, including their own, with $\eta_{ij}\, g_{\text{syn}} = 22$ nS. The scaling η_{ij} for the strength of inhibition from the LN of glomerulus j onto the PNs of glomerulus i are given by the Pearson correlation coefficient of the activity of the two glomeruli in response to 16 odourants as observed in the experimental data of Ditzen (2005). The use of correlation-dependent connectivity was motivated by the work of Linster et al. (2005) that has demonstrated that the amplitude of lateral interactions within the AL are governed more by correlations of glomerular activation patterns than by anatomical proximity of the glomeruli. An additional reason for this choice over homogeneous strength of inhibition was our hypothesis that different active LNs should lead to different PN activation patterns. This would not be the case if all LNs exerted the same pattern of inhibition onto the LN population.

In our practical model implementation the 600 ORNs projecting to each glomerulus are simulated by 15 "compound ORNs" with 40-fold higher firing rates hence exploiting the additivity of Poisson processes for obtaining more efficient simulations.

2.8. Simulation

The model was simulated with custom C++ code which is published along with the paper at modelDB (`http://senselab.med.yale.edu/modeldb/`). We used a 6/5 order variable time step Runge Kutta algorithm with maximal time step of 0.1 ms to integrate the equations.

2.9. Data Analysis

Data from the simulations was analysed in custom C++ software and Matlab (Mathworks Inc.) scripts.

As will become clear in the results section below, the direct inspection of glomerular activity in terms of the averaged SDF of the PNs of each glomerulus allows only limited insights into the meaning of the observed activity patterns. In order to elucidate the relevance of the activity patterns, we used correlation analysis and principle component analysis (PCA).

We first analysed individual trials with different stimulus conditions in correlation maps, where we plot the correlation between each glomerular activation pattern over time with the activation pattern in response to the same or other stimuli at all other times. This illustrates the similarity of individual responses to different stimulus conditions, e.g. the similarity of the response to a single odour with the response to a mixture stimulus, and in a fully time-resolved manner.

However, to provide an overview of how similar the response to any given stimulus is to the typical response to a single odour or the typical response to the synchronous mixture, we investigated the average correlation of the response of interest with "response templates". The response templates were calculated from the response to each of the single odours and to the synchronous mixture. To form a response template, we averaged the SDF of all 5 PNs in each glomerulus in the time window 100-200 ms after stimulus onset. This provides a 30-dimensional vector of the typical activation levels of the 30 modelled glomeruli which then is correlated with the instantaneous response vectors in response to other stimuli. In the results we report the observed correlations between templates and responses averaged over 10 independent trials.

Finally, in order to provide an illustration of the relationship between the responses to different stimuli independent of correlations (and the involved normalisation of responses) we also calculated a PCA reduction of the 30-dimension PN activity space. These PCA plots in figure 7 were produced by using the Matlab `princomp` function on SDF data that was averaged for all 5 PNs in each glomerulus. We used the first 200 ms of the response to all conditions for calculating principal components. We then applied `rotatefactors` to implement a Varimax rotation. The entire response trajectories and the template vectors (large round markers in figure 7) were subsequently transformed into the resulting PCA coordinates.

3. Results

3.1. AL response patterns in response to single odours

The first goal of the model was to reproduce the observed glomerular response patterns in the AL using a realistic olfactory receptor model. We used reaction rate equations for the binding and unbinding of odourants at the receptors (see Methods) and adjusted the rate constants in the equations iteratively in order to match the average spike density function (SDF) of PNs in the model to the experimentally observed Ca^{2+} activation patterns (Ditzen,

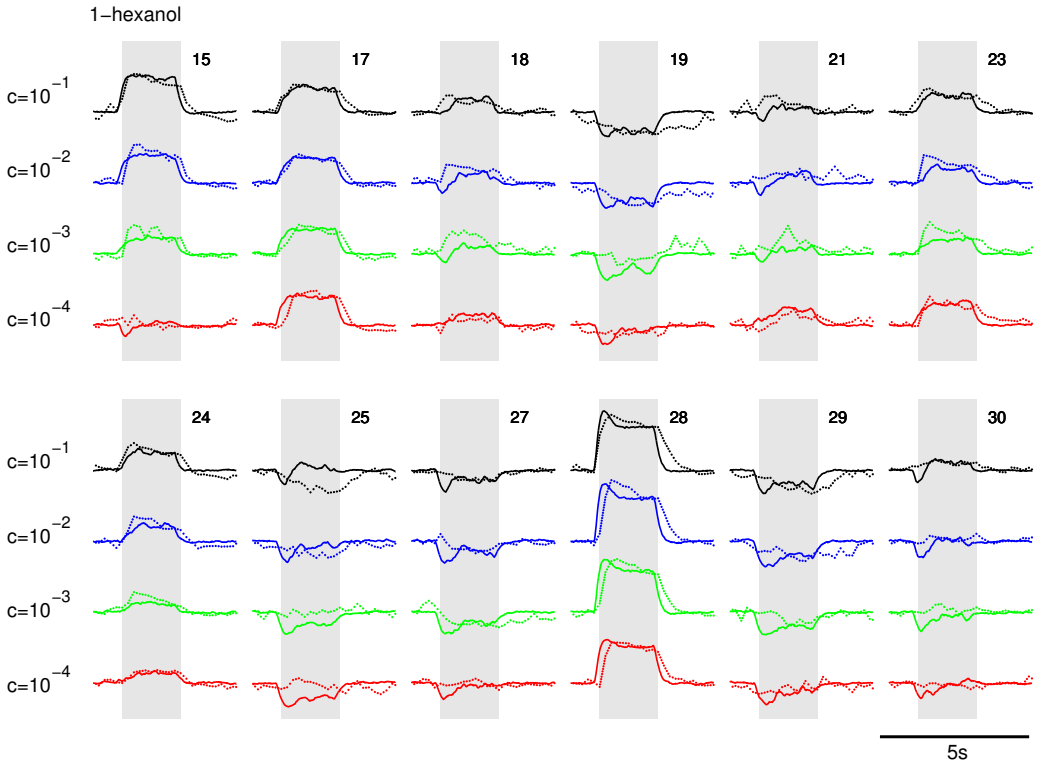

Figure 2: Response profiles to H for 12 exemplary glomeruli in the imaging data (dotted lines) and the model data (solid lines). The imaging data represents relative change in fluorescence normalised to the range $[-1, 1]$ and the model data are spike density functions (SDF) of PN spike trains, generated with an asymmetric kernel of width 50 ms, also normalised to $[-1, 1]$ around the average baseline firing rate. The colour code indicates responses to dilutions 10^{-4} (red), 10^{-3} (green), 10^{-2} (blue) and 10^{-1} (black). The numbers in each sub-panel denote the number of the glomerulus according to the standardised bee AL atlas (Galizia et al., 1999). The grey bars mark the 2s presence of the hexanol stimulus. The full set of fitted data for all 16 odourants and all 30 considered glomeruli is displayed in the supplementary material.

2005). Figure 2 illustrates the achieved correspondence between experimental and modelling data for the odourant 1-hexanol. The complete data that was used to reproduce realistic glomerular activation patterns and the resulting matching model data are shown in the supplementary text. The odourants 1-hexanol (subsequently referred to as H) and 1-nonanol (subsequently referred to as N) have previously been used in behavioural and physiological experiments on asynchronous mixture coding in honeybees (Szyszka et al., 2012; Stierle et al., 2013). The responses to 4 odourant concentrations (see colour code in the caption of figure 2) in 30 glomeruli that are well-accessible to Ca^{2+} imaging have been used. The used glomeruli are indicated in figure 1 by semi-transparent shells. The match of experimental data and model activity is overall satisfactory with a few small exceptions: (i) Some glomeruli exhibit long tails of slowly decaying activity that is not implemented in the model, (ii) the model exhibits a fast transient inhibition in glomeruli that overall receive balanced excitation and inhibition (e.g. glomerulus 19 at concentration 10^{-4} in figure 2) that stems from a strong phasic response of LNs that decays rapidly due to spike rate adaptation in ORNs and LNs. The absence of rapid inhibition in the calcium imaging data may be due to the fact that a reduction in action potential frequency does not always result in a reduction of intra-cellular calcium concentration Galizia and Kimmerle (2004).

3.2. Response patterns to mixtures

After matching the response to individual odourants to the experimental data we proceeded to simulate the response to synchronous and asynchronous mixtures. The model was exposed to individual odourants H and N at a concentration of 10^{-2} for 800 ms per odourant and responses were saved. Then, the model was exposed to 800 ms of the synchronous mixture and to stimulations with asynchronous mixtures with delays 6, 50 and 200ms between odour onsets.

The responses of PNs to the H-6-N mixture and N-6-H mixture differ and the H-6-N mixture response is quite different from the HN response while the N-6-H and HN responses are quite similar to each other (supplementary figure S1). This can be explained from inspecting the activity of LNs (figure 3). As explained in the methods, LNs strongly inhibit each other, which implements a winner-take-all (WTA) type attractor network where only the LN of the most strongly activated glomerulus is active and suppresses the activity in all other LNs. The odour inputs H and H-6-N typically activate the LN of glomerulus 28 and the odour inputs N, HN and N-6-H typically activate the LN of glomerulus 33. Hence, the same LN is active in the HN and N-6-H input condition, leading to the very similar response patterns in these two conditions, while different LNs are active for H-6-N and HN, which makes the responses quite different. The same activation patterns are observed for the H-200-N and N-200-H conditions (figure 3B). As expected, the response

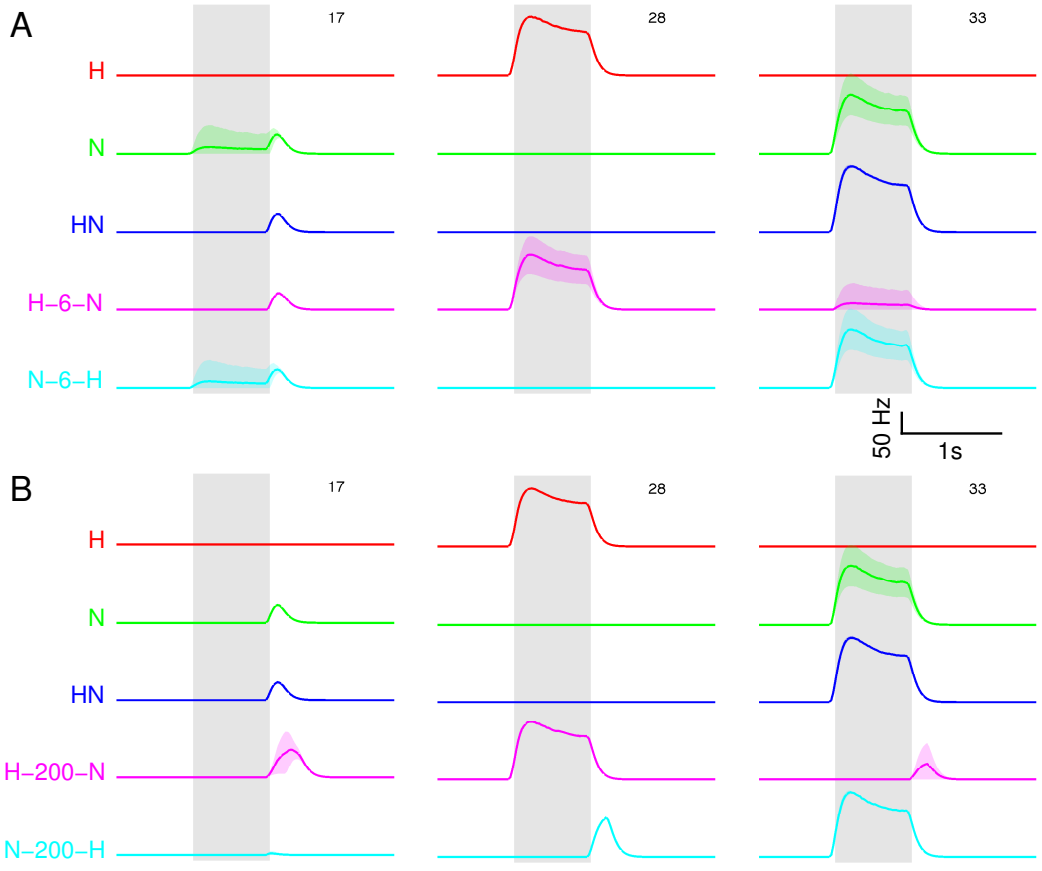

Figure 3: LN responses in the glomeruli 17, 28 and 33 to the five stimulus conditions of H, N, synchronous mixture HN and asynchronous mixtures H-6-N, N-6-H (A) and H-200-N, N-200-H (B). We plotted the average spike density function observed in 10 independent trials plus/minus one standard deviation. The coloured patches of non-zero standard deviation indicate that in some trials by chance the winning LN is different. This is particularly true for the 6 ms delays. All other LNs that are not shown here are essentially silent due to the lateral inhibition between LNs.

reliability of the dominant LNs is increased for the longer delay as evidenced by the smaller standard deviations of the responses.

3.3. Correlations between response patterns

To quantify our observations and determine how responses relate to each other, in particular when allowing for an overall scaling of the response amplitude, we performed two types of correlation analysis. We first calculated the full delayed auto- and cross-correlation matrices between responses (figures 4A-F, 5) in a single trial. Then, for an overall assessment of response similarities we calculated correlation functions between responses and typical response templates (figure 4G and figure 6, see Methods for details).

The auto-correlations of responses to H, N and HN (figure 4A,D,F) show that the response patterns are stable, i.e. highly correlated with themselves throughout the stimulation and for an additional 100-200 ms after stimulus offset. The latter effect is likely caused by the asymmetric SDF kernel (see Methods) that will "smear out" responses beyond their offset. The response to H lingers somewhat longer after stimulus offset and then the correlations rapidly decline, while the transition is a little earlier but more gradual for N and HN. Furthermore, both N and HN exhibit a marked post-odour response (figure 4D,F arrowheads) which is stable for about 300 ms and not particularly similar in its response pattern to the initial responses. The cross-correlation map between N and HN indicates that this after-response is highly correlated for the response to N and the response to HN. During the initial main response, the HN responses are first briefly more similar to the N response, then slightly more similar to the H response. It is only in the after-response, that the HN response becomes very correlated with the N response.

We observe consistent effects in the template analysis (figure 4G). The responses to H, N and the synchronous mixture HN are very strongly correlated to their own response template throughout the response. Furthermore, the next-highest correlations are between the single odourant templates and the synchronous mixture response, with the lowest correlations between the H and N responses, confirming the impression from comparing figure 4B to C and E. We note that during most of the response the synchronous mixture appears to be equally similar to the N template and the H template.

In the cross-correlations of response patterns to responses evoked by asynchronous mixtures (figure 5) the effect of the LN network becomes apparent. The response to the asynchronous mixture H-6-N appears to be most similar to the N response for the whole duration of the stimulus (figure 5B) and to a lesser degree similar to the HN response (figure 5C). And it is similarly correlated to the off-responses to N and HN. The correlation to the H response is markedly lower throughout (figure 5A) and the 6 ms period of H being present on its own is so brief that it is invisible.

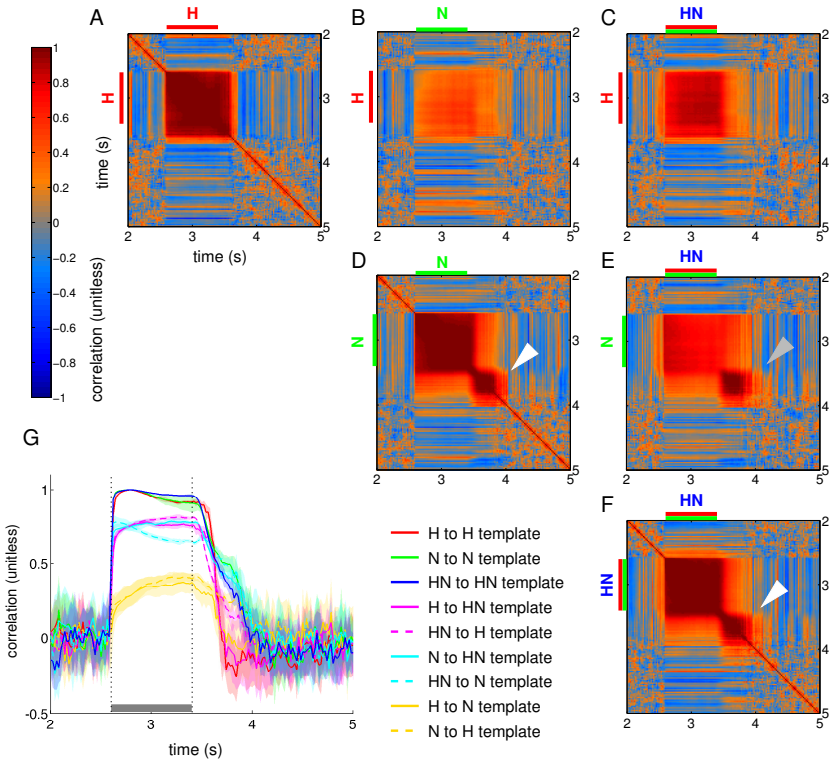

Figure 4: Correlation maps between the responses to the single odourants and the synchronous mixture (A-F). The colour maps show the correlation of the vector of average PN SDF values of all glomeruli with the same vector for a different time (auto-correlation maps A,D,F) or with the response SDF vectors for a different input (cross-correlation maps B,C,E). The involved odourants are marked by the coloured stimulation bars (H in red and N in green). In the auto-correlation maps the correlations are strong (close to 1) throughout the stimulation and for about 100-200 ms afterwards. For N and the synchronous mixture HN, there is also an post-odour response of about 300 ms duration (white arrowheads in D,F) which is correlated with itself for this duration but less correlated with the initial response. The post-odour responses for N and HN are also strongly correlated with each other (grey arrowhead in E). G) Correlation curves of the single odourants and the synchronous mixture with each other's response templates. The lines are the mean of the observed correlation in 10 independent runs and the shaded areas demarcate plus/minus one standard deviation around the mean (capped at 1). Note how each response is most similar to its own response template, next most similar are single odourants with the synchronous mixture and the least correlated are the single odourants with each other.

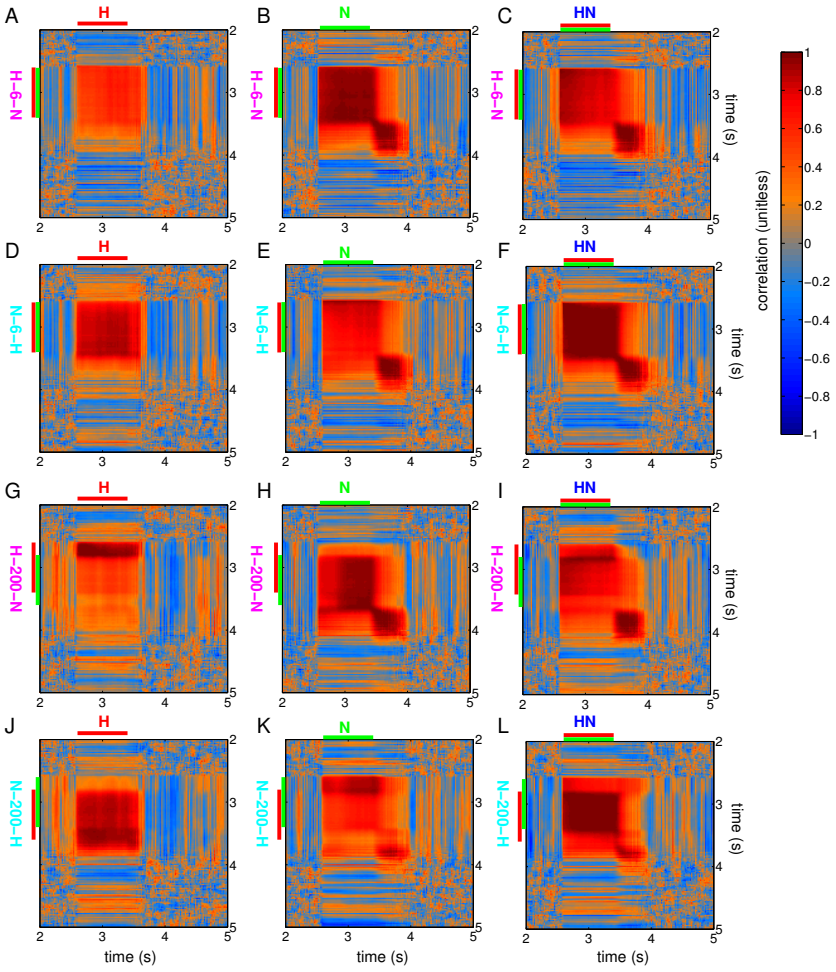

Figure 5: Cross-correlation maps of the asynchronous mixtures H-6-N (A-C), N-6-H (D-F), H-200-N (G-I) and N-200-H (J-L) with the responses to H, N and HN. The presence of the stimuli is indicated by the coloured bars (H in red and N in green). Correlations were calculated for a single run of each stimulus condition using the average SDF of the PN population of each glomerulus at 20 ms time steps.

These findings are confirmed by the average template response similarities (figure 6A). the response to the H-6-N mixture is equally similar to the N template and the HN template, and less to the H template. This may be surprising at first as one would expect that the initial presence of H would activate the H-specific LN activity (which it does, see figure 3) and hence induce an H-type activity pattern. However, the inhibition pattern exerted by the H-specific LN does not necessarily make an activity pattern look more H-like, if it is applied to an activity pattern that is not elicited by H. For example, due to the choice of correlation-based connectivity, the inhibition of the H-specific LN_{28} onto the most activated glomerulus for H, also glomerulus 28, is strong. This will attenuate the activation of glomerulus 28 whenever LN_{28} is active which can actually make an activity pattern look *less H-like*.

For the N-6-H response the situation is slightly different (figure 5D-F). Here, as we know already, the activated LN is LN_{33}, i.e. the N- and HN-activated LN. Accordingly, as for almost the entire stimulus H and N are present and the HN specific LN is on, N-6-H is most correlated with the HN response and less so with the N or the H responses. The same is observed in the average correlations to response templates (figure 6B). Interestingly, between the correlations to the H and N responses, N-6-H seems to first correlate a bit stronger to the N response, and then to the H response. In the post-odour response N-6-H is again more N-like than H-like, but clearly also HN-like.

For the longer 200 ms delay mixtures, we see the emergence of clearly visible initial and final phases where the H-200-N mixture correlates first for about 200 ms with the H response (figure 5G, 6C) and then correlates mainly with the N response (figure 5H) like for the short delay mixture H-6-N. In the post-odour response H-200-N is equally strongly correlated to the N and HN responses.

Similarly, the N-200-H response is first strongly correlated to the N response for about 200 ms (figure 5K, 6D) and then becomes most correlated to the synchronous mixture response (figure 5L). However, as for the N-6-H mixture, if we compare the correlations of N-200-H to the H and N responses during the main body of the stimulation, it appears to be more correlated to the H than to the N response. For the N-200-H response, there is a 200 ms period at the end of the stimulation where the similarity to the H response dominates and this curtails the typical N- and HN-like post-odour response seen in the other cases.

3.4. Dependence on the choice of OR kinetics

The results reported in the previous section may depend on the particular receptor kinetics that we derived through our bootstrapping procedure from single odour responses observed in Ca^{2+} imaging data. As we have discussed in the methods section, the receptor kinetics that best fit the data are only loosely constrained such that there are many similarly good fits. As a simple

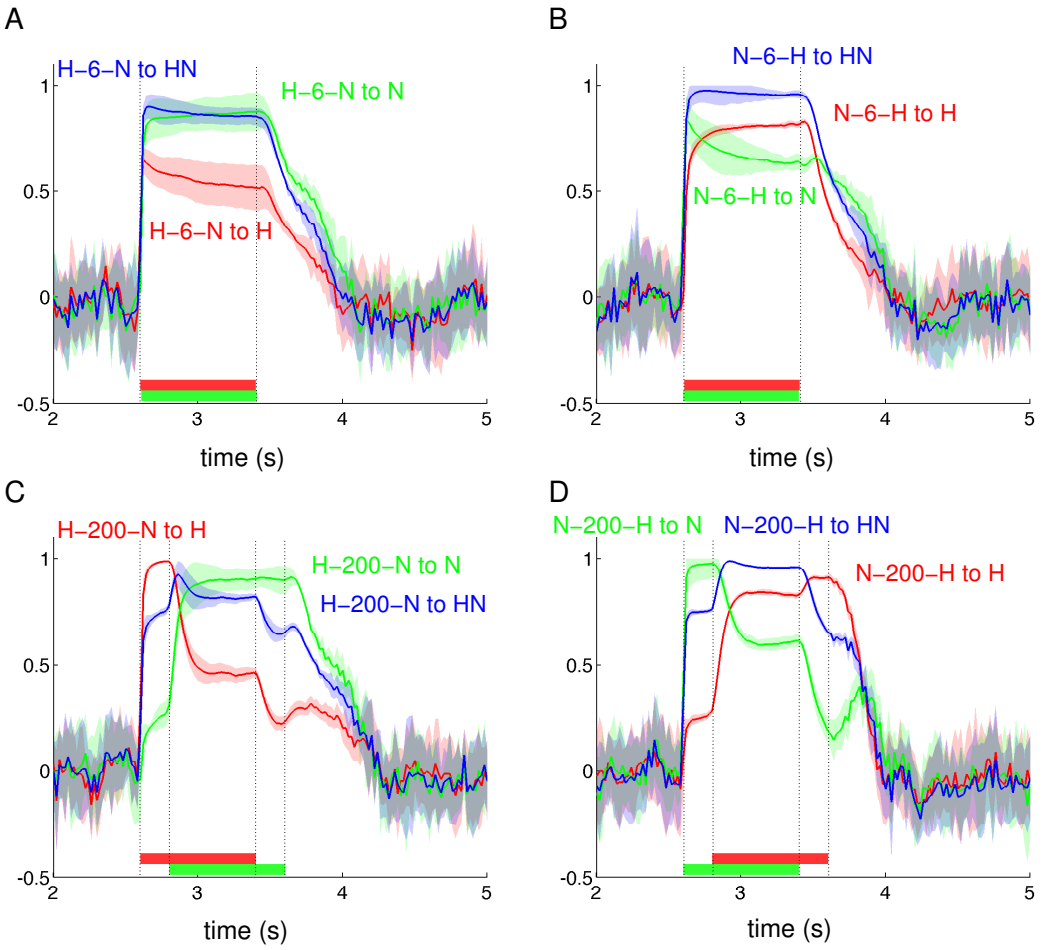

Figure 6: Correlation analysis of the responses to pure odours, the synchronous mixture and asynchronous mixtures. The correlation analysis was performed for asynchronous mixtures with 6 ms delay (A,B) and 200 ms delay (C,D). The lines are the mean of the observed correlation in 10 independent runs and the shaded areas demarcate plus/minus one standard deviation around the mean (capped at 1).

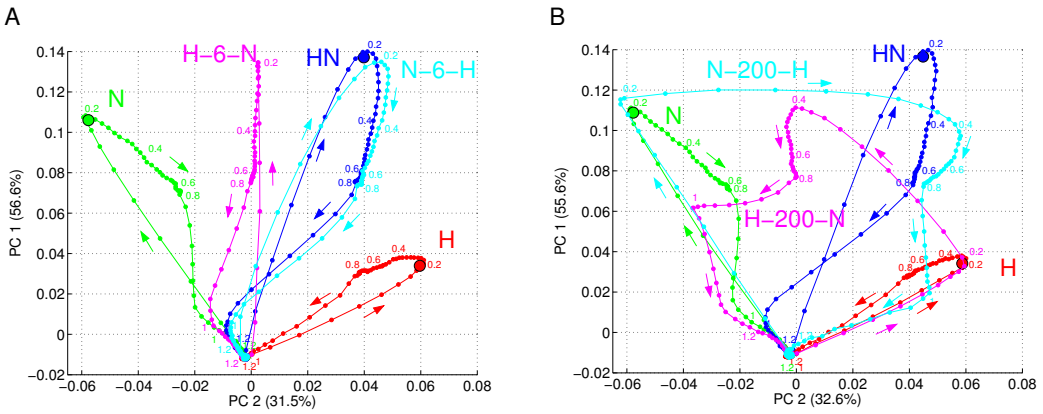

Figure 7: Illustration of the responses to individual odourants and different mixture conditions, with 6 ms delay (A) and 200 ms delay (B), in the first two components of a PCA transformation. The PCA was applied to the initial 200 ms of PN SDF activity patterns sampled at 20 ms time steps and the time in seconds from stimulus onset is annotated along the trajectories. The percentage of overall variance captured by the components is noted in brackets on the axes. The trajectories are the average trajectories from 10 independent runs of the model. Note how the trajectories for the asynchronous mixtures for the 200 ms delay (B) are first similar to the early odourant and then cross-over to a mixture representation. The late response then is similar to the trailing odourant in the mixture. When the mixture representation is realised, i.e. when both mixture components are present, the N-t-H mixtures are very similar to HN, while the H-t-N mixture occupies an area between the HN and N trajectories.

control for whether our results hold more generally, we repeated the simulations of H, N, HN, H-t-N, and N-t-H mixtures with a different set of the receptor kinetic parameters that was of a similar quality as our original set used throughout this paper. We found that the results were essentially identical with only small differences in the correlation values (see supplementary figure S3).

3.5. Principal component analysis of responses

To further dissect our results and relate them to our concurrent experimental work (Stierle et al., 2013) but also previous work in locust (Broome et al., 2006) we visualised the 30 dimensional response patterns by the first two principle components (Figure 7). The N-6-H response is almost identical to the HN response and its template whereas the H-6-N response is between the N response and the HN response, explaining the comparable correlation values to either of them. For the longer delay of 200 ms, we see an interesting cross-over in the responses to asynchronous mixtures, which first follow the trajectory of the leading odourant and then switch over to either the N trajectory (H-200-N mixture) or to the synchronous mixture HN trajectory (N-200-H mixture). At the end the trajectories then follow the trajectory of the response to the trailing odourant. This corresponds well to similar results reported by Broome et al. (2006) in the locust and our observations

in experiments (see figure 6 in (Stierle et al., 2013)).

3.6. Separability of the entire odour set

As we have fitted the responses to all 16 odourants in the Ditzen data set (Ditzen, 2005), we can perform simulations and make predictions for any combination of odourants in this set, not only H and N. We asked for which odour pairs the responses to asynchronous mixtures would be different from those to the corresponding synchronous mixtures like we observed for H and N so far. In order to find out we simulated the responses to all possible pairs of odourants in delayed mixture assays and automatically identified the correlations of delayed mixtures X-6-Y with X, Y and XY template responses for all odourants X, and Y (see figure 8).

To quantify how the asynchronous mixture responses relate to the responses to the individual odourants in comparison to how they relate to the response to the synchronous mixture, we calculate the correlation ratio of the correlations of the corresponding response templates. This takes the form of the leading odourant correlation ratio

$$\mathrm{CR}_{\mathrm{lead}}(t,T) = \frac{c(a_{\text{X-t-Y}}(T), \overline{a}_{\mathrm{X}})}{c(a_{\text{X-t-Y}}(T), \overline{a}_{\mathrm{XY}})} \tag{15}$$

and the trailing odourant correlation ratio

$$\mathrm{CR}_{\mathrm{trail}}(t,T) = \frac{c(a_{\text{X-t-Y}}(T), \overline{a}_{\mathrm{Y}})}{c(a_{\text{X-t-Y}}(T), \overline{a}_{\mathrm{XY}})} \tag{16}$$

where $c(.,.)$ denotes the Pearson correlation coefficient, $a_{\text{X-t-Y}}(T)$ the average activity pattern evoked by the X-t-Y input during T to $T + 100$ ms after stimulus onset, and $\overline{a}_{\mathrm{X}}, \overline{a}_{\mathrm{Y}}, \overline{a}_{\mathrm{XY}}$ the usual response templates for inputs X, Y, and their synchronous mixture XY. If $\mathrm{CR}_{\mathrm{lead}}(T)$ is greater than 1, then the response pattern to the asynchronous mixture is more similar to the response template of the early odourant, and if it is smaller than 1 it is more similar to the response template of the synchronous mixture. Similarly, $\mathrm{CR}_{\mathrm{trailing}}(T) > 1$ indicates larger correlations with the trailing odourant's response template than with the synchronous mixture template and $\mathrm{CR}_{\mathrm{trailing}}(T) < 1$ vice versa.

We evaluated the correlation ratios in the early response ($T = 100$ ms), main response ($T = 700$ ms) and post-odour response ($t = 900$ ms). For the short delay X-6-Y mixtures, there are only a few odour pairs where the correlations between the asynchronous mixture and one of the components are considerably higher than the correlations of the asynchronous mixture with the synchronous mixture (red squares in figure 8A-C indicating $\mathrm{CR}_{\mathrm{lead}} > 1$). However, there is a tendency that towards the end of the stimulation the X-6-Y response is more correlated with the X template than with the XY template (figure 8C). However, a word of caution may be in order here. As we

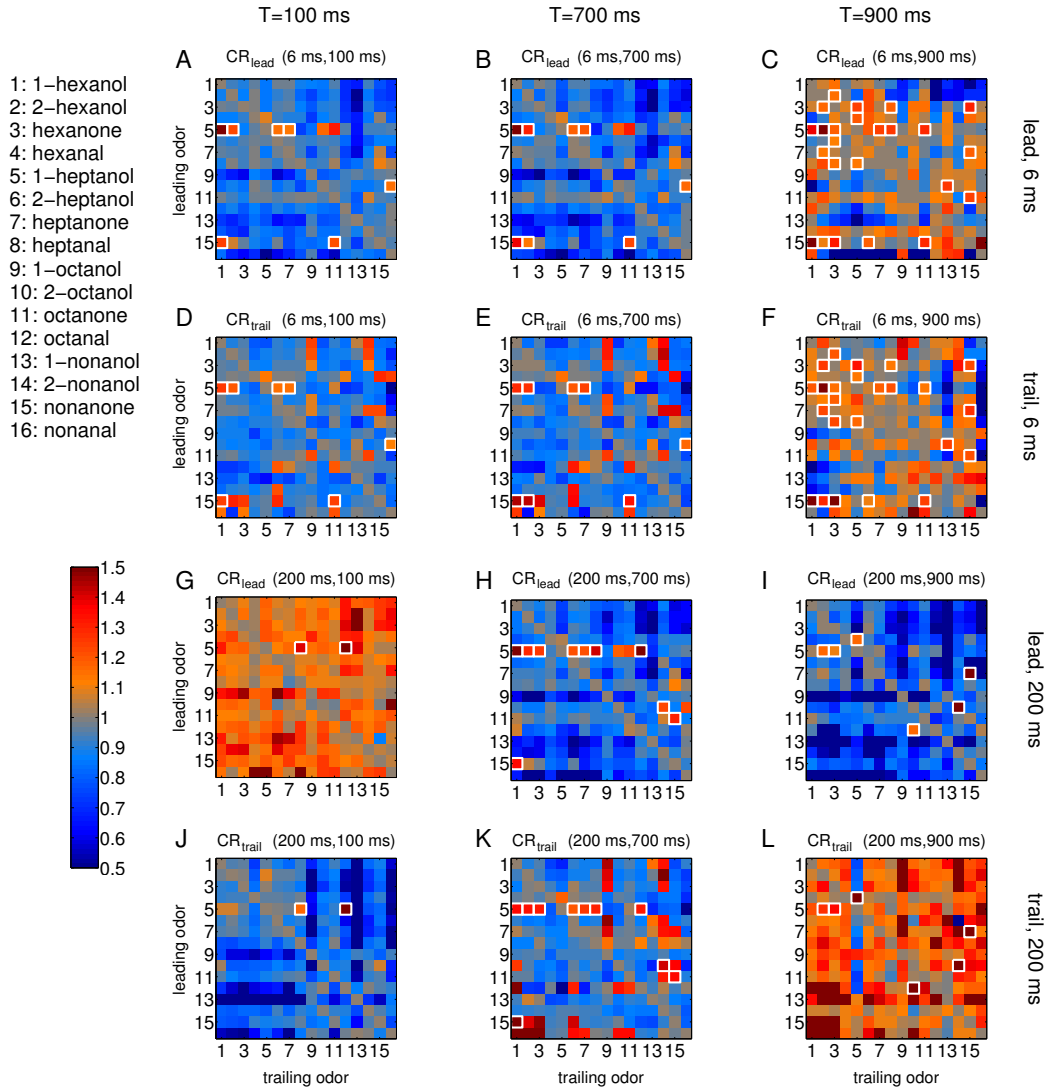

Figure 8: Correlation ratios of the leading and trailing odourant of all possible binary mixtures of the 16 considered odourants. (A-C) Red colour indicate that the X-6-Y response is more correlated to the X response template than to the synchronous mixture response template. A blue colour indicates on the contrary that the response to X-6-Y is more similar to the synchronous mixture response template. (D-E) The same analysis A-C is performed but comparing the correlations with the Y response to the correlations with the synchronous mixture response. (G-I) and (J-L) show the same analysis for X-200-Y delayed mixtures. Note that depending on odour pairing the asynchronous mixture either looks more like the leading or more like the trailing odourant, or, in many cases, more like the synchronous mixture (blue colours). In some cases (e.g. 1-heptanol with 1-octanol), the response to the asynchronous mixture is more similar to the template response of one of the odourants (octanol) no matter which one comes first, and in other cases it is not (e.g. 1-heptanol and nonanal). For the short delay panels (A-F), there is a tendency that the single odourant templates "shine through" in the late response (more red colours in C,F). For the long delay mixtures we observe the expected effect that the leading odourant is correlated with the early response in the asynchronous mixture (G) and the trailing odourant correlates with the late response (L). The white boxes highlight odour pairings for which the response to the incoherent mixture is more similar to *both* the responses to the leading and trailing odourants than to the response to the synchronous mixture.

are inspecting a ratio of correlations, the overall strength of the correlations is lost and may be low.

For longer delays we observed, as expected, that the asynchronous X-200-Y mixture generally looks initially more like X (figure 8H) and in the late response more like Y (figure 8L). In the middle of the response (figure 8H,K) the distribution of similarities is very similar to the X-6-Y case. This is due to the fact that the same LNs will be activated in both cases and the same syntopic mixture model will be applied such that the overall response should be similar in both X-6-Y and X-200-Y conditions during the time where both odour components are present.

4. Discussion

Behavioural experiments in bees have shown that synchronous binary odour mixtures can be processed in a synthetic way, i.e. they have a perceptive quality that is to some degree different from their components (Chandra and Smith, 1998; Smith, 1998; Deisig et al., 2003; Lachnit et al., 2004; Gerber and Ullrich, 1999). However, stimulus-onset asynchrony of only 6 ms between two components of a binary mixture enables bees to distinguish the asynchronous mixture from the synchronous mixture and to better segregate components from the mixture (Szyszka et al., 2012). If conditioned to respond to H or N, they subsequently show a higher probability to respond to the asynchronous mixtures H-6-N and N-6-H than to the synchronous mixture HN (Szyszka et al., 2012). Consistent with this observation, the PN responses in the AL, as seen in calcium imaging (Stierle et al., 2013), are sensitive to millisecond stimulus asynchrony. These observations do, however, not fully explain the symmetric behavioural data as asynchronous mixtures always appear to be dominated by one of the component odours in the physiological data. Here we set out to offer a possible explanation for PN sensitivity to millisecond onset-asynchrony between odourants using computational modelling. Given the short timescale of 6 ms of the minimal necessary odour onset delay, compared to the ms timescale of spikes, several ms timescale of synaptic transmissions and 5 ms timescale of minimal observed inter-spike-intervals, it seems very unlikely that any behavioural relevant activity could be processed within the 6 ms where only a single odourant is present. Moreover, behavioural studies showed that odour sampling times shorter than 500 ms reduce honeybees ability to recognise and discriminate odours Wright et al. (2009); Fernndez et al. (2009). Rather, we hypothesised, the short time t where the stimulus is different between H-t-N and HN or N-t-H and HN must lead to a more prolonged change in the evoked activity during the remaining stimulation which then can be exploited behaviourally. In the model this effect persists for the entire period in which both H and N stimuli are present, i.e. for 794 ms (for the 6 ms delay) and 600 ms (for the 200 ms delay).

A similar effect has been demonstrated in the auditory system of humans, where a tone that is added to a mixture of tones is perceived as separate if its onset is delayed, while it is perceived as part of the overall tone if its onset is synchronous (Lipp et al., 2010). In this analogue of asynchronous sound mixtures, the perception of the separate tone also persists throughout the stimulus. If, as we hypothesised and as our model suggests, the response pattern to an asynchronous odour mixture in the AL of honeybees remains different throughout the stimulus duration, the difference could be significant enough to be exploited behaviourally.

4.1. Attractor network of LNs

We have put forward an attractor network of local neurons as a candidate mechanism for achieving a prolonged change of the evoked activity in response to an asynchronous stimulus. In particular, we have investigated a model in which the local neurons in the antennal lobe form a WTA competitive inhibitory network. When stimulated by an odourant the most excited LN will commence to fire first and with the highest rate and through lateral wide-field inhibitory connections suppresses the activity in all other LNs. This condition will remain stable (an attractor) until the stimulus changes drastically enough for a different LN to escape inhibition and be the "winner" or until the stimulus subsides and the LNs fall silent.

Our simulations demonstrate that under realistic assumptions (amplitude and type of noise in ORNs, number of ORNs, and the resulting convergence ratio of 600:1 of ORNs to LNs), the circuit will rather reliably activate odour-specific "winner" LNs in good agreement with the results of Zavada et al. (2011). Furthermore, we observed that a delay of only 6 ms in an asynchronous mixture was sufficient to reliably activate the winning LN of the leading odourant and the activation of this LN persisted for the duration of the stimulus (see figure 3). It is noteworthy that smaller convergence ratios do not allow this mechanism to be sufficiently reliable down to such short delays (data not shown).

4.2. LN network connectivity

The LNs in the AL inhibit the PNs in a pattern that has been shown to likely be related to the correlations between glomerular activations (Linster et al., 2005). Here, we have incorporated this into the model by choosing the maximal inhibitory conductance of LN-PN synapses proportional to the correlation between the activation of the corresponding glomeruli as observed in the Ditzen data set (Ditzen, 2005) (see Methods). Accordingly, the pattern of inhibition exerted by the LNs onto the PNs in the AL is different for each LN, such that a different winning LN will lead to a different modification of the overall excitation pattern of PNs in the AL. It is this effect that generates the different activation patterns in response to asynchronous mixtures and, as we hypothesise, the ability to distinguish them from each

other and the synchronous mixture. Whether the particular connectivity pattern based on correlations of glomerular activation used in this study is the most effective for separating the responses to asynchronous mixtures is an open question that can be addressed in the model but necessitates extensive numerical exploration including repeated costly bootstrapping of receptor response profiles. We will address this question elsewhere.

4.3. Different effects for different mixture components

In the example of H and N used in the behavioural and physiological experiments (Szyszka et al., 2012; Stierle et al., 2013), and used for comparison throughout this paper, the winning LNs for H (LN in glomerulus 28) and N (LN in glomerulus 33) differ, but the winning LN for the synchronous mixture HN is the same as the winning LN for N. Therefore, the asynchronous mixture H-t-N, which will activate LN_{28}, has a markedly different activation pattern than HN, while the N-t-H pattern has the same winning LN_{33} as HN and hence looks very similar to the HN pattern during the time where both odourants are present in the mixture. In this example of H and N, hence, the symmetry breaking effect of the LN network is effective for H-t-N mixtures but less so for N-t-H mixtures. From our overall scan of all possible odour pairings within the odourant set of 16 odours available to us, this situation seems typical (Figure 8). We see that in many of the cases where there is a change in similarity away from the synchronous mixture, it is only for one of the odourants. Interestingly, this odourant does not need to be the leading odourant in the asynchronous mixture. Already in our main H and N example, the asynchronous H-t-N mixtures are more similar to N in the main response window than they are to H. At first this may seem surprising because it is the H specific LN_{28} which wins (see figure 3). However, on closer inspection it is clear that the response pattern of PNs depends on many factors, not only the currently active LN. First of all, the PN response pattern is determined by the ORN responses to the mixture. These are described with our syntopic mixture model which is known to reproduce non-trivial mixture interactions on the receptor level (Rospars et al., 2008; Münch et al., 2013). Then, this ORN activation pattern is modified by the PN response characteristics and eventually the inhibition from the currently active LN_{28}. It is by no means clear that the inhibition pattern of the H-specific LN_{28} will render a mixture response to look more like an H response. On the contrary, because the assumed correlation-dependent inhibition pattern includes considerable self-inhibition of the most active glomerulus 28 one can expect at least the response of this glomerulus to be suppressed and the PN activation pattern therefore to be *less H-like* because of it.

In the overall picture of all odour pairs we observe that there are odour pairings like H and N where the asynchronous mixture is more similar to the trailing odourant. But there are also examples other than H and N where the similarity of the asynchronous mixture is increased towards the leading

odourant. Furthermore, there are a few examples, even though a minority, where the asynchronous mixture is more similar to both of the components than to the synchronous mixture (figure 8, white boxes). Therefore, the WTA dynamics in the LN network does not necessarily segregate the first odour to arrive, but in a network model based on real physiological data only takes effect for some specific odours (figure 8). Thus, the network connectivity in the AL favours some odours against others, a property that will benefit the animal if these odours are of greater ecological significance.

For larger delays we find that, as expected, the response first looks like the response to the leading odourant alone, then similar to an asynchronous mixture response with the features just described, and then similar to the response to the trailing odourant alone. In asynchronous mixtures with such long delay the bees would likely be able to recognise the components in the asynchronous mixture, independent of the hypothesised mechanism of the LN network activity.

4.4. Comparison to physiological data

In a companion work (Stierle et al., 2013) we have performed optical recordings using Ca^{2+} dyes in the AL of bees and analysed the similarity between PN response patterns to H, N, HN, H-t-N and N-t-H stimuli directly. Like in the model we found that one asynchronous mixture is more similar to one of the odourants and the reverse order asynchronous mixture is most similar to the synchronous mixture. This is consistent with the effect of having two distinct winning LNs of which one is shared by the synchronous mixture and one of the components. Interestingly, however, the roles of H and N appear to be reversed in the experiments compared to the model. In the experimental observations the H-t-N mixtures are more similar to H whereas they are more similar to N in the model. The N-t-H mixture, however, is most similar to the synchronous mixture HN in both. One possible explanation for the partial mismatch of model predictions and experimental observations is that the model was based on a different experimental data set and hence that the responses to H and N were not fully consistent with the newer data. Reason for the experimental variability could be differences in the dye (Oregon Green versus Fura-2), staining method (dye-injection between the mushroom body calyces versus laterally to the alpha lobes), in the temperature (28°C versus room temperature) and in the dynamics and concentration of the odour stimuli.

Another source of inconsistency between the model and the imaging data can be the employed mixture model. While recent work (Münch et al., 2013) has demonstrated that syntopic mixture models (Rospars et al., 2008) are highly successful in predicting the interaction of odourants at receptors, it is well-known that additional interactions between odourants can occur on the receptor or neuron level (Nikonov and Leal, 2002; Hillier and Vickers, 2011; Su et al., 2012). Inaccuracies in the model predictions for the synchronous and

asynchronous mixture responses based on mixture interactions not captured by our syntopic mixture model could easily lead to a change in the dominance of any of the components in the mixture and hence the slightly different results.

Furthermore, as discussed above, the assumed connectivity of LNs onto PNs was based on previous observations of a numerical analysis of the interactions of glomeruli as observed in imaging data (Linster et al., 2005) but has by no means been established as the ground truth for the AL of the bee. The pattern of LN inhibition onto PNs plays an important role in determining the PN activation pattern and hence the details of the similarity of asynchronous mixtures to either of their components. We also have neglected LNs other than homogeneous GABAergic wide-field LNs which provide inhibition across the whole AL (see Methods). Other LN types could well play a role in shaping the exact response pattern of PNs as well.

Summarising this part, we believe that we have constructed a model to the best of our current knowledge of the bee olfactory system although we had to incorporate quite a few assumptions. The model is consistent with the principal findings in physiological experiments (Stierle et al., 2013) and although it fails when making more detailed predictions, we see it as a good starting point for further investigations. Based on this model and its rooting in experimental data we can make concrete predictions that can be compared to experiments; if the predictions fail, like for aspects of the H and N dominance discussed here, this information can be used to construct future refined models that approximate the system increasingly well. For example, future models could be calibrated on a single consistent data set for single odours and mixtures rather than on the two partially inconsistent experimental data sets of Ditzen (2005) and Stierle et al. (2013) used here. Further refinements could also come from fitting the connectivity within the AL to reproduce synchronous mixture responses rather than assuming the correlation-based connectivity used here and predicting such responses from single odourant data.

4.5. Predicted effect of blocking inhibition

Based on our model we can make the prediction that blocking inhibition in the AL should remove the odour segregation ability of bees for asynchronous mixtures with short delays while leaving the ability intact of distinguishing mixtures with longer delays from synchronous mixtures. To test this hypothesis in the model, we simulated the removal of inhibition by setting the synaptic conductance of LN to PN connections to 0. As expected, the responses to H-6-N and N-6-H are now virtually indistinguishable from the synchronous mixture response (supplementary figure S4) and when analysing the similarity to H and N response templates, they only differ in that H-6-N is a little more similar to the H template and N-6-H is a little more similar to the N template for a very short time at stimulus onset (arrowheads in

supplementary figure S4). For longer delays of 200 ms, however, the initial similarity to the leading odour and the similarity to the trailing odour at stimulus offset are clearly visible independent of the presence of inhibition (compare figures 6 and S4). Based on our simulations and the analysis with response templates as in figures 6 and S4, the boundary between short and long delay mixtures, when a visible correlation to the leading odour appears to become more pronounced in the initial response, is around 20 ms delay (data not shown).

In earlier work on learning odour recognition in insects (Huerta et al., 2004; Nowotny et al., 2005; Huerta and Nowotny, 2009) we have suggested and successfully employed the idea that odour patterns are processed within discrete 50 ms "snapshots" in the mushroom bodies and higher brain areas in the insect brain. Under that hypothesis, asynchronous mixtures of less than 50 ms onset delay would depend on the LN network activity to disambiguate between asynchronous and synchronous mixtures, pushing the predicted onset delays where asynchronous mixture recognition becomes inhibition-independent to at least 50 ms.

5. Conclusions

Our model has demonstrated that under reasonable assumptions, a WTA inhibitory LN network can lead to a symmetry breaking effect where the response to an asynchronous mixture is noticeably different from the response to the synchronous mixture for an extended period beyond the timescale of the odour onset delay. This effect can prevail down to 6 ms delays and offers a possible explanation for the ability of the insect olfactory system to distinguish asynchronous mixtures with very short delays.

6. Acknowledgements

This work was supported by the Engineering and Physical Sciences Research Council (grant number EP/J019690/1) to TN and the Bundesministerium für Bildung und Forschung (grant number 01GQ0931) to PS and CGG.

7. Supplementary figure captions

Figure S1: PN responses in the asynchronous mixture experiment with 6 ms delay. Responses were simulated for 10 independent trials and averaged. The coloured regions demarcate plus/minus one standard deviation from the mean response in the 10 trials. Note how the responses to the H-6-N mixture are different to single odourant responses and different to the synchronous mixture responses, while the N-6-H responses follow closely the HN responses.

Figure S2: PN responses in the asynchronous mixture experiment with 200 ms delay. The data was prepared and is presented as in figure S1. Note the sometimes drastic changes in activity after 200 ms stimulation when the second odour arrives.

Figure S3: Repeated numerical experiment of similarities between responses to H, N, HN, H-t-N and N-t-H with a different set of parameters for receptor kinetics from our bootstrapping procedure. Note that the described effects are all well conserved (cf figure 6). The most salient difference, if any, is that the H-6-N response is a bit closer to the N response than to the HN response in this scenario.

Figure S4: Response similarities of responses to H, N, HN, H-t-N and N-t-H in the absence of inhibition in the AL. When the inhibition is absent, the responses to H-6-N and N-6-H are almost identical except for a very brief period at stimulus onset (arrowheads). In this brief period, the correlation of the response to H-6-N to the H response template is larger than the correlation of the response to N-6-H this template. After a few milliseconds, however, both responses are exactly the same. Furthermore, during the entire duration of the stimulus the responses to asynchronous mixtures are most similar to the synchronous mixture, and less similar to the single odourants.

References

Abel, R., Rybak, J., Menzel, R., 2001. Structure and response patterns of olfactory interneurons in the honeybee *Apis mellifera*. J Comp Neurol 437, 363–383.

Andersson, M.N., Binyameen, M., Sadek, M.M., Schlyter, F., 2011. Attraction modulated by spacing of pheromone components and anti-attractants in a bark beetle and a moth. J Chem Ecol 37, 899–911. URL: http://dx.doi.org/10.1007/s10886-011-9995-3, doi:10.1007/s10886-011-9995-3.

Baker, T.C., Fadamiro, H.Y., Cosse, A.A., 1998. Moth uses fine tuning for odour resolution. Nature 393, 530.

Broome, B., Jayaraman, V., Laurent, G., 2006. Encoding and decoding of overlapping odor sequences. Neuron 51, 467–482.

Buckley, C.L., Nowotny, T., 2011. Multiscale model of an inhibitory network shows optimal properties near bifurcation. Phys Rev Lett 106, 238109.

Chandra, S., Smith, B.H., 1998. An analysis of synthetic processing of odor mixtures in the honeybee (apis mellifera). J Exp Biol 201, 3113–3121.

Deisig, N., Lachnit, H., Sandoz, J.C., Lober, K., Giurfa, M., 2003. A modified version of the unique cue theory accounts for olfactory compound processing in honeybees. Learn Mem 10, 199–208. URL: http://dx.doi.org/10.1101/lm.55803, doi:10.1101/lm.55803.

Destexhe, A., Mainen, Z.F., Sejnowski, T.J., 1994. An efficient method for computing synaptic conductances based on a kinetic model of receptor binding. Neural Comput 6, 14–18.

Ditzen, M., 2005. Odor concentration and identity coding in the antennal lobe of the honeybee Apis mellifera. Ph.D. thesis. Freie Universität Berlin. Berlin.

Fernndez, V.M., Arenas, A., Farina, W.M., 2009. Volatile exposure within the honeybee hive and its effect on olfactory discrimination. J Comp Physiol A Neuroethol Sens Neural Behav Physiol 195, 759–768. URL: http://dx.doi.org/10.1007/s00359-009-0453-4, doi:10.1007/s00359-009-0453-4.

Galizia, C.G., 2008. Insect olfaction, in: D. V. Smith, S. Firestein, G.K.B. (Ed.), The senses, a comprehensive reference. Elsevier, London, pp. 725–769.

Galizia, C.G., Kimmerle, B., 2004. Physiological and morphological characterization of honeybee olfactory neurons combining electrophysiology, calcium imaging and confocal microscopy. J Comp Physiol A 190, 21–38.

Galizia, C.G., McIlwrath, S.L., Menzel, R., 1999. A digital 3D atlas of the honeybee antennal lobe based on optical sections acquired using confocal microscopy. Cell Tissue Res 295, 383–394.

Gerber, Ullrich, 1999. No evidence for olfactory blocking in honeybee classical conditioning. J Exp Biol 202 (Pt 13), 1839–1854.

Hammer, M., 1997. The neural basis of associative reward learning in honeybees. Trends Neurosci 20, 245–252.

Hillier, N.K., Vickers, N.J., 2011. Mixture interactions in moth olfactory physiology: examining the effects of odorant mixture, concentration, distal stimulation, and antennal nerve transection on sensillar responses. Chem Senses 36, 93–108. URL: http://dx.doi.org/10.1093/chemse/bjq102, doi:10.1093/chemse/bjq102.

Hopfield, J.J., 1991. Olfactory computation and object perception. P Natl Acad Sci USA 88, 6462–6466. URL: http://www.pnas.org/cgi/content/abstract/88/15/6462.

Huang, J., Zhang, W., Qiao, W., Hu, A., Wang, Z., 2010. Functional connectivity and selective odor responses of excitatory local interneurons in Drosophila antennal lobe. Neuron 67, 1021–1033. URL: http://dx.doi.org/10.1016/j.neuron.2010.08.025, doi:10.1016/j.neuron.2010.08.025.

Huerta, R., Nowotny, T., 2009. Fast and robust learning by reinforcement signals: Explorations in the insect brain. Neural Comput. 21, 2123–2151.

Huerta, R., Nowotny, T., Garcia-Sanchez, M., Abarbanel, H.D.I., Rabinovich, M.I., 2004. Learning classification in the olfactory system of insects. Neural Comput 16, 1601–1640.

Krofczik, S., Menzel, R., Nawrot, M.P., 2008. Rapid odor processing in the honeybee antennal lobe network. Front Comput Neurosci 2, 9. URL: http://dx.doi.org/10.3389/neuro.10.009.2008, doi:10.3389/neuro.10.009.2008.

Lachnit, H., Giurfa, M., Menzel, R., 2004. Odor processing in honeybees: is the whole equal to, more than, or different from the sum of its parts? Adv. Study Behav. 34, 241–264.

Linster, C., Sachse, S., Galizia, C.G., 2005. Computational modeling suggests that response properties rather than spatial position determine connectivity between olfactory glomeruli. J Neurophysiol 93, 3410–3417. URL: http://dx.doi.org/10.1152/jn.01285.2004, doi:10.1152/jn.01285.2004.

Lipp, R., Kitterick, P., Summerfield, Q., Bailey, P.J., Paul-Jordanov, I., 2010. Concurrent sound segregation based on inharmonicity and onset asynchrony. Neuropsychologia 48, 1417–1425. URL: http://dx.doi.org/10.1016/j.neuropsychologia.2010.01.009, doi:10.1016/j.neuropsychologia.2010.01.009.

Münch, D., Schmeichel, B., Silbering, A.F., Galizia, C.G., 2013. Weaker ligands can dominate an odor blend due to syntopic interactions. Chem Senses URL: http://dx.doi.org/10.1093/chemse/bjs138, doi:10.1093/chemse/bjs138.

Murlis, J.J., Elkinton, Cardé, R.T., 1992. Odor plumes and how insects use them. Annual Review of Entomology 37, 505–532.

Nikonov, A.A., Leal, W.S., 2002. Peripheral coding of sex pheromone and a behavioral antagonist in the Japanese beetle, Popillia Japonica. J Chem Ecol 28, 1075–1089.

Nowotny, T., Huerta, R., Abarbanel, H.D.I., Rabinovich, M.I., 2005. Self-organization in the olfactory system: Rapid odor recognition in insects. Biol Cyber 93, 436–446.

Nowotny, T., Rabinovich, M.I., 2007. Dynamical origin of independent spiking and bursting activity in neural microcircuits. Phys Rev Lett 98, 128106.

Olsen, S.R., Bhandawat, V., Wilson, R.I., 2007. Excitatory interactions between olfactory processing channels in the Drosophila antennal lobe. Neuron 54, 89–103. URL: http://dx.doi.org/10.1016/j.neuron.2007.03.010, doi:10.1016/j.neuron.2007.03.010.

Riffell, J.A., Lei, H., Christensen, T.A., Hildebrand, J.G., 2009. Characterization and coding of behaviorally significant odor mixtures. Curr Biol 19, 335–340. URL: http://dx.doi.org/10.1016/j.cub.2009.01.041, doi:10.1016/j.cub.2009.01.041.

Rospars, J.P., Lansky, P., Chaput, M., Duchamp-Viret, P., 2008. Competitive and noncompetitive odorant interactions in the early neural coding of odorant mixtures. J Neurosci 28, 2659–2666. URL: http://dx.doi.org/10.1523/JNEUROSCI.4670-07.2008, doi:10.1523/JNEUROSCI.4670-07.2008.

Rybak, J., 1994. Die strukturelle Organisation der Pilzkörper und synaptische Konnektivitt protocerebraler Interneuronen im Gehirn der Honigbiene, Apis mellifera. Eine licht- und elektronenmikroskopische Studie. Ph.D. thesis. Freie Universität Berlin.

Sachse, S., Galizia, C.G., 2002. Role of inhibition for temporal and spatial odor representation in olfactory output neurons: A calcium imaging study. J Neurophysiol 87, 1106–1117.

Shang, Y., Claridge-Chang, A., Sjulson, L., Pypaert, M., Miesenböck, G., 2007. Excitatory local circuits and their implications for olfactory processing in the fly antennal lobe. Cell 128, 601–612. URL: http://dx.doi.org/10.1016/j.cell.2006.12.034, doi:10.1016/j.cell.2006.12.034.

Silbering, A.F., Galizia, C.G., 2007. Processing of odor mixtures in the Drosophila antennal lobe reveals both global inhibition and glomerulus-specific interactions. J Neurosci 27, 11966–11977. URL: http://dx.doi.org/10.1523/JNEUROSCI.3099-07.2007, doi:10.1523/JNEUROSCI.3099-07.2007.

Silbering, A.F., Okada, R., Ito, K., Galizia, C.G., 2008. Olfactory information processing in the Drosophila antennal lobe: anything goes? J Neurosci 28, 13075–13087. URL: http://dx.doi.org/10.1523/JNEUROSCI.2973-08.2008, doi:10.1523/JNEUROSCI.2973-08.2008.

Smith, B.H., 1998. Analysis of interaction in binary odorant mixtures. Physiol Behav 65, 397–407.

Stierle, J.S., Galizia, C.G., Szyszka, P., 2013. Millisecond stimulus onset-asynchrony enhances information about components in an odor mixture. Journal of Neuroscience 33, 6060–6069. doi:10.1523/JNEUROSCI.5838-12.2013.

Strauch, M., Ditzen, M., Galizia, C.G., 2012. Keeping their distance? odor response patterns along the concentration range. Front Syst Neurosci 6, 71. URL: http://dx.doi.org/10.3389/fnsys.2012.00071, doi:10.3389/fnsys.2012.00071.

Su, C.Y., Menuz, K., Reisert, J., Carlson, J.R., 2012. Non-synaptic inhibition between grouped neurons in an olfactory circuit. Nature 492, 66–71. URL: http://dx.doi.org/10.1038/nature11712, doi:10.1038/nature11712.

Szyszka, P., Stierle, J.S., Biergans, S., Galizia, C.G., 2012. The speed of smell: odor-object segregation within milliseconds. PLoS One 7, e36096. URL: http://dx.doi.org/10.1371/journal.pone.0036096, doi:10.1371/journal.pone.0036096.

Traub, R.D., Miles, R., 1991. Neural Networks of the Hippocampus. Cambridge University Press, New York.

Vosshall, L.B., Wong, A.M., Axel, R., 2000. An olfactory sensory map in the fly brain. Cell 102, 147–159.

Witthöft, W., 1967. Absolute Anzahl und Verteilung der Zellen im Hirn der Honigbiene. Z Morphol Tiere 61, 160–184.

Wright, G.A., Carlton, M., Smith, B.H., 2009. A honeybee's ability to learn, recognize, and discriminate odors depends upon odor sampling time and concentration. Behav Neurosci 123, 36–43. URL: http://dx.doi.org/10.1037/a0014040, doi:10.1037/a0014040.

Yaksi, E., Wilson, R.I., 2010. Electrical coupling between olfactory glomeruli. Neuron 67, 1034–1047. URL: http://dx.doi.org/10.1016/j.neuron.2010.08.041, doi:10.1016/j.neuron.2010.08.041.

Zavada, A., Buckley, C.L., Martinez, D., Rospars, J.P., Nowotny, T., 2011. Competition-based model of pheromone component ratio detection in the moth. PLoS One 6, e16308. URL: http://dx.doi.org/10.1371/journal.pone.0016308, doi:10.1371/journal.pone.0016308.